Dynamics of pairwise motions in the fully nonlinear regime in LCDM and modified gravity cosmologies

Mariana Jaber,[1,*] Wojciech A. Hellwing,[1] Jorge E. García-Farieta,[2,3] Suhani Gupta,[1] and Maciej Bilicki[1]

[1]*Center for Theoretical Physics, Polish Academy of Sciences, Al. Lotników 32/46, 02-668 Warsaw, Poland*
[2]*Instituto de Astrofísica de Canarias, s/n, E-38205, La Laguna, Tenerife, Spain*
[3]*Departamento de Astrofísica, Universidad de La Laguna, E-38206, La Laguna, Tenerife, Spain*

(Received 1 December 2023; accepted 16 May 2024; published 14 June 2024)

In contrast to our understanding of density field tracers, the modeling of direct statistics pertaining to the cosmic velocity field remains open to significant opportunities for improvement. The lack of accurate modeling for the nonlinear domain of pairwise velocities restricts our capacity to fully exploit the information encoded in this observable. We present a robust approach for modeling the mean infall velocities, $v_{12}(r,a)$, with broad applicability spanning sub-megaparsec scales and cosmologies extending beyond the standard ΛCDM paradigm. Our approach involves solving the full pair-conservation equation using accurate nonlinear power spectrum descriptions. To assess the robustness of our model, we extend it to cosmologies beyond the standard ΛCDM, in particular, the Hu-Sawicki $f(R)$-gravity and Dvali-Gabadadze-Porrati (DGP) modified gravity models. Remarkably, our predictions for pairwise velocities of dark matter particles at kiloparsec scales exhibit excellent agreement with N-body simulations throughout the entire dynamical range ($0.1 \lesssim \xi \lesssim 1000$, or $r \geq 0.4h^{-1}$ Mpc). Furthermore we show that different gravity models leave distinct signatures in the shape and dynamics of the mean pairwise velocities, providing a potent test of cosmological gravity laws.

DOI: 10.1103/PhysRevD.109.123528

I. INTRODUCTION

Pairwise velocities and the large-scale velocity fields serve as crucial statistics for the large-scale structure (LSS), offering valuable insights that complement the widely utilized density-based measurements. However, unlike our understanding of cosmic density, the modeling and understating of direct statistics of the cosmic velocity field still have considerable room for improvement. This deficiency is one of the main reasons why the rich information encoded in the velocity field and its potential as a cosmological probe is still largely untapped.

Various approaches have been employed to model the nonlinear regime of structure formation in the density field. These include the standard perturbation theory (SPT) (see [1–5]), regularized perturbation theory [6], fitting formulas like Halofit and HMCODE (see [7–9]), and emulator approaches (see e.g. [10–13]).

As we delve into the small-scale features of the Universe, it becomes increasingly vital to harness the complementary information embedded in peculiar velocity fields. Pairwise velocities, measuring the typical relative velocity between objects at specific separations, contain information about the peculiar motions induced by gravity. As such the information encoded in the moments of the pairwise velocity distribution may be considered as crucial for modeling and deciphering the nonlinear regime.

The velocity field data has been already effectively utilized in various applications, including redshift-space distortions (RSD) growth-rate estimates (for instance [14,15]), bulk-flow measures ([16]), cosmic web analysis (see [17]), measuring the velocity power spectrum (e.g. [18]), or in field reconstructions (see [19,20] or [21] where the authors reconstruct the density and velocity fields using [22], the most recent update to the cosmic flows catalog [23]).

In the late 1970s, a potent method for modeling mean pairwise velocities (MPV) emerged [24–27]. This approach led to the application of the Bogoliubov-Born-Green-Kirkwood-Yvon (BBGKY) hierarchy of equations, which describe the dynamic evolution of self-gravitating particle systems, for modeling of the large-scale cosmic velocity fields. Within this hierarchy, the first moment is known as the pair-conservation equation [25,26], represented as:

$$\frac{\partial \xi}{\partial t} + \frac{1}{x^2 a}\frac{\partial}{\partial x}[x^2(1+\xi)v] = 0. \tag{1}$$

It expresses the conservation of particle pairs separated by a comoving distance x in terms of the two-point correlation function (2PCF) of density fluctuations, $\xi(x,t)$, and the relative velocity of pairs, v. Here, t denotes cosmological time, and a stands for the scale factor.

*jaber@cft.edu.pl

The result derived from Eq. (1) was employed by [28] to propose an interpolation-based ansatz for the mean pairwise velocity (MPV), bridging the gap between linear and nonlinear regimes, and improving the results proposed by [29]. The physical reason behind the coefficients of [28]'s fitting formula was later explained in [30] and extended to treat galaxies in [31].

The BBGKY formalism was used to constrain the cosmic matter density parameter $\Omega_{\rm M}$ (as seen in [32]) and for testing cosmological models, including those with nonzero curvature [28]. However, its performance significantly deteriorates on highly nonlinear scales.

MPVs capture the dynamics of peculiar motions driven by gravitational interactions in an expanding background Universe. This sensitivity has motivated research efforts aimed at using MPVs to identify deviations from GR in large-scale structure formation (as demonstrated in [33–38]). The absence of precise modeling for the nonlinear regime of pairwise velocities hinders our ability to fully harness the physical information inherent in this observable.

In this paper, we introduce a precise modeling approach for pairwise velocities. Our primary focus lies in enhancing predictions on nonlinear scales. We validate our predictions against N-body simulations, and show the versatility and strength of this modeling, by stress-testing it for nonstandard cosmologies such as modified gravity (MG) scenarios.

We aim to construct our model using well-established and readily available methodologies rather than introducing new analytical or numerical tools. By demonstrating the effective application of these methods for precise predictions on sub-megaparsec separations, we seek to provide the community with a robust framework for modeling MPVs and using them to test the underlying gravity model.

This paper is organized as follows: in Sec. II we review the pair conservation equation, describe the models for nonlinear scales included in our work and our simulation data. In Sec. III we present our results for the MPV in ΛCDM and for MG scenarios, which we discuss in Sec. IV and we present our main conclusions in Sec. V.

II. METHODS

We proceed to describe the analytical models, numerical techniques and simulation data we used to build and test our pairwise velocity modeling.

A. Model

Our model for computing the mean pairwise velocities, $v_{12}(x,a)$, relies in the consistent numerical solution of the following equation [28]:

$$\frac{a}{3[1+\xi(x,a)]}\frac{\partial\bar{\xi}(x,a)}{\partial a}=-\frac{v_{12}(x,a)}{H(a)r} \tag{2}$$

where $\bar{\xi}(r,a)=3x^{-3}\int_0^x\xi(y,a)y^2dy$ is the volume-averaged 2PCF, $H(a)$ is the Hubble function, and $r=ax$ is the proper separation between pairs.

Before describing the different approaches for the nonlinear clustering, let us briefly examine the limiting values of Eq. (2). In the case of pairs separated at $x\ll 1h^{-1}$ Mpc or, equivalently, high values of $\xi\gg 1$ we recover the *stable clustering* regime. This regime consists of scales where the natural tendency of a pair to collapse, as induced by the gravitational clustering, dominates over the background Hubble expansion, thus a regime where the term $(v_{12}(r)+Hr)$ is negative. The opposite case, i.e., at large x where $\xi(x,t)\ll 1$, is known as the *linear regime* (see for e.g. [27]). Here the growing mode of structure formation dominates and we have $\xi(r,t)=D(t)^2\xi(r,t=0)=D(t)^2\xi_0(r)$, with which we get:

$$v_{12}(x,a)=-\frac{2}{3}axHf\bar{\bar{\xi}}(x,a), \tag{3}$$

where $\bar{\bar{\xi}}(x,a)\equiv\bar{\xi}(x,a)/[1+\xi(x,a)]$ and f is the logarithmic derivative of the growth function, $f\equiv d\ln D/d\ln a$. It is important to recall that the splitting of $\xi(r,t)$ in a time, $D(t)$, and a space dependent function, $\xi_0(r)$, requires that the linear growth function is scale independent, which is generally satisfied in the GR and nDGP cases.

An essential aspect is the transition point where the influence of the Hubble flow on large scales gives way to the stable clustering regime at smaller separations, and then further into the virialized regime, where the orbits inside the collapsed haloes are essentially randomized. These transitions are of particular significance, especially when considering cosmologies with different growth-rate histories, such as MG theories.

B. Modified gravity

In our study, as a way of stress-testing our model, we include non-ΛCDM cosmologies. In particular, we explore MG models as extensions to ΛCDM. These MG theories introduce alterations to the standard framework, leading to distinct phenomenological consequences that are relevant for our research. Specifically, we focus on two MG theories:

(1) The normal branch of the Dvali-Gabadadze-Porrati (nDGP) model. This theory seeks to explain the accelerated expansion of the universe by introducing extra dimensions that influence gravity on large scales while preserving standard general relativity (GR) at small scales. It does so by introducing a scalar field, called the brane-bending mode, which influences the gravitational interaction on large scales. This modification allows for a departure from standard gravitational laws at cosmic distances. [39].

(2) The Hu-Sawicki form of $f(R)$-gravity [40]. This widely adopted extension of the Hilbert-Einstein

action introduces a functional dependence of the Ricci scalar, R, within the Einstein-Hilbert equations, which characterizes the curvature of spacetime. The function $f(R)$ allows for variations in the gravitational force as a function of the curvature so that this modification aims to explain cosmic acceleration without invoking dark energy (for a review see for instance [41,42]).

To deviate from GR on cosmological scales while respecting both high-density and strong-field regime constraints, these MG theories introduce "screening mechanisms." These mechanisms are theoretical concepts designed to reconcile the predictions of MG with experimental observations on cosmological and astrophysical scales, effectively concealing modifications to Einstein's field equations in various environments (the regime of high densities or small distances). The first family illustrates the Vainshtein screening mechanism [43], implemented in the nDGP gravity model. The Vainshtein mechanism relies on the nonlinearity of equations of motion for the scalar field, leading to a suppression of its effects at small scales. On the other hand, the specific form of $f(R)$ gravity we consider employs the Chameleon screening mechanism [44]. In the Chameleon mechanism, a scalar field possesses a variable effective mass dependent on local matter density, allowing it to be screened in high-density environments while remaining active in low-density regions. For a thorough review on this type of theories we refer the reader to [45].

C. Data

For calibration and testing the pairwise-velocity model, we use data generated from the suite of DM-only MG N-body simulations: ELEPHANT (Extended Lensing Physics using Analytic ray Tracing), [46], as these simulations provide a good test-bed to study the impact of both the Chameleon and Vainshtein screening mechanisms on the large scale nonlinear clustering of matter.

This set of N-body simulations assumes a ΛCDM background, and implements on top of this the solution of the scalar field and modified Einstein equations in the MG models described above: normal branch of the DGP theory, or nDGP, and the Hu-Sawicki form of $f(R)$. In the first case, the specific values of the extra parameter are $Hr_c = 1, 5$ (referred to as N1 and N5, respectively), and for the second model, the strength of the modification is codified by the present-day value of the derivative of the $f(R)$ function, $|f_{R,0}|$, taking the values 10^{-5}, and 10^{-6} (referred to as F5 and F6, respectively). N1 codifies a model that deviates more strongly from GR than N5, in a similar way just as F5 deviates more from GR than F6.

For each model and redshift, we have five independent realizations. The different MG models have the same fiducial ΛCDM background. For a detailed explanation of the numerical parameters used in this suite of simulations we refer the reader to Sec. 2.2 from [47].

For the direct calculation of the pairwise velocities in the simulation data, we use the positions and velocities of the dark-matter particles and analyse the snapshots at $z = 0$, 0.3 and 0.5.

D. Nonlinear power spectrum

To model the MPV accurately for sub-Mpc separations, we must address the nonlinear clustering component in Eq. (2). To achieve this, we employ various proposals for the nonlinear power spectrum, denoted as $P_{\rm nl}(k, z)$. These $P_{\rm nl}(k, z)$ are subjected to an inverse Fourier transform (IFT) to provide the corresponding nonlinear two-point correlation function (2PCF), denoted as $\xi_{\rm nl}(r, a)$, as required in Eq. (2).

Nonlinear clustering in ΛCDM: In our study, we test and employ the Halofit solution which is implemented in the cosmological Boltzmann solver CAMB [48,49]. We fix the cosmological parameters to the values of the ELEPHANT simulations. The Halofit formula is an accurate fitting formula for the nonlinear matter power spectrum, presented in [50] and recalibrated in [8]. We choose to use the Halofit model for the ΛCDM case due to its established accuracy, tested to be up to ∼5% for $k \leq 10h^{-1}$ Mpc, and $z \leq 2$, for a variety of ΛCDM and wCDM cosmologies (see for instance [8]).

Additionally, we also compare our results against the solution from the Convolution Lagrangian Perturbation Theory (CLPT) [51], which is a nonperturbative resummation of Lagrangian perturbation theory and provides as an output, an estimation for $v_{12}(r, a)$.

Nonlinear clustering in modified gravity: In the context of MG scenarios, which deviate from the standard paradigm, there is less consensus on the optimal approach for modeling the nonlinear power spectrum. Various proposals exist, some of which compute it directly using N-body simulations [52,53], perturbation theory [54], post-Friedman formalism (PPF) [55], or via the spherical collapse model [56]. Specifically for $f(R)$ gravity, a MG version of the standard Halofit, known as "MG-Halofit," has been introduced [57]. It is essential to note that these approaches are based on certain assumptions and have limitations, which restrict their applicability and generality. Instead, we primarily utilize the following two tools: the standard Halofit solution and MGCAMB[1] [58], a modified version of CAMB specifically designed to handle both the $f(R)$ and nDGP gravity models. Our choice of background cosmology remains consistent between the ΛCDM and MG cases, aligning with the setup of the ELEPHANT simulations. Consequently, the primary differences between GR and the MG models manifest in the growth of perturbations. It is important to stress that the version of Halofit that we use is agnostic to MG as it was developed and tested for ΛCDM and wCDM cosmologies [8]. An in-depth exploration of

[1]https://github.com/HAWinther/FofrFittingFunction.

the limitations to model the nonlinear $P(k)$ for MG models can be found in [59]. However, and as we will demonstrate in following sections, albeit its lower precision to model nonlinear $P(k)$ in MG models, is already enough for getting percent-level predictions for $v_{12}(r,a)$.

For a quick comparison with our MGCAMB + Halofit solutions, we also include a recent approach proposed by [59] to compute the nonlinear matter power spectrum in the context of MG. This work introduces a nonlinear matter power spectrum for MG, $P_{\rm nl,MG}(k,z)$, in terms of a ΛCDM nonlinear power spectrum, $P_{\rm nl,\Lambda CDM}(k,z)$, and a halo model response function, $\Upsilon(k,z)$, which has been calibrated against the ELEPHANT suite of simulations. The resulting power spectrum as function of scale, k, and redshift, z, $P_{\rm nl,MG}(k,z)$ can be expressed as:

$$P_{\rm nl,MG}(k,z) = \Upsilon(k,z) \times P_{\rm nl,\Lambda CDM}(k,z), \tag{4}$$

where $\Upsilon(k,z)$ represents a function that encapsulates the power deviation of ΛCDM concerning the specified MG model. For $P_{\rm nl,\Lambda CDM}(k,z)$ in Eq. (4), we also employed the Halofit prediction from CAMB, consistent with the cosmological parameters used in the ELEPHANT simulations. The specific components of the halo model for MG were detailed in [59], where the authors report a 5% accuracy up to nonlinear scales of $k \lesssim 2.5$–$3h^{-1}$ Mpc in their resulting power spectra.

III. RESULTS

In this section, we present the outcomes of our study, which revolves around the modeling of MPVs in the nonlinear regime. To achieve this, we utilize the previously mentioned methodologies for computing the nonlinear matter power spectrum and solve for $v_{12}(r,a)$ using Eq. (2). Our presentation begins with a focus on the ΛCDM model, followed by an exploration of the applicability of our MPV model in the context of MG scenarios.

A. MPV for the ΛCDM model

Figure 1 displays the solution for Eq. (2) for ΛCDM across different panels. Moving from top to bottom, we present the MPV, denoted as $v_{12}(r,a)$ in units of km s^{-1}, at varying redshift values. The panels labeled with their redshift value: $z = 0, 0.30.5$, encompass our findings for separations ranging between $r \in 0.05$–$140h^{-1}$ Mpc, shown in linear scaling, allowing us to cover both the linear and nonlinear regimes simultaneously. Below these, we zoom in on the region $r \in 0.05$–$40h^{-1}$ Mpc, now in logarithmic x-axis scaling, providing a more detailed view of our solution's behavior in the nonlinear regime. Finally, the panels marked with Δv_{12}, also in logarithmic x-axis scaling, depict the ratio of our numerical solution for $v_{12}(r,a)$ with respect to the simulation data, represented as $\Delta v_{12} \equiv (v_{12} - v_{12,\rm sim})/v_{12,\rm sim}$. The simulation MPVs, $v_{12,\rm sim}(r)$, are determined directly calculating the projected velocity differences of pairs of dark matter particles. These simulation results are indicated by black dots, with error bars illustrating the variance across five independent realizations of each snapshot.

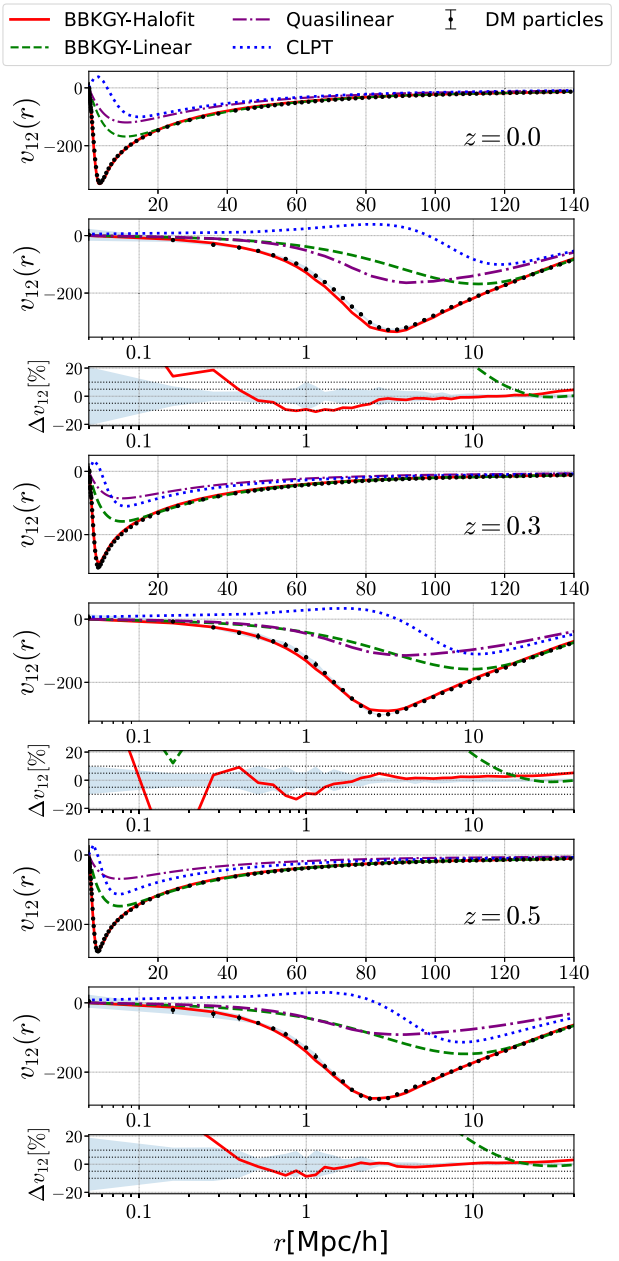

FIG. 1. Pairwise velocity models for DM tracers, $v_{12}(r,a)$, in units of km s^{-1} and for the ΛCDM cosmology. Points correspond to velocities from ELEPHANT runs, lines correspond to the different theoretical models: the full solution to Eq. (2) using the linear CAMB matter power spectrum (dashed green), solution obtained via nonlinear Halofit based power spectrum (solid red), the quasilinear approximation given by eq. Eq. (3) (dot-dashed purple), and the prediction from CLPT (dotted blue).

To obtain numerical solutions for $v_{12}(r,a)$, we utilize Eq. (2) with specific prescriptions. We employ the nonlinear output from Halofit, represented by red solid lines labeled as "BBKGY-Halofit." We also include the linear power spectrum from CAMB, shown as green dashed lines and labeled as "BBKGY-linear." To facilitate comparison with the results of [28], we present a solution to Eq. (3) using the Halofit power spectrum as input, indicated by purple dot-dashed lines and labeled as the "quasilinear" solution. Lastly, we include the solution for $v_{12}(r,a)$ obtained from the numerical implementation of the convolution Lagrangian perturbation theory (CLPT),[2] providing the real-space pairwise in-fall velocity in units of $v/aH(a)f$. These results are represented by the dotted blue lines.

It is worth noting the agreement among all the solutions for separations $r \geq 80h^{-1}$ Mpc. This agreement is expected since these scales fall well within the linear regime, where the dynamics of pairwise velocities are primarily driven by the Hubble expansion. It is important to mention that the results from CLPT were originally optimized for galaxy clustering analysis, specifically for extracting the baryonic acoustic oscillations (BAO) feature from the 2PCF of biased tracers. As a result, CLPT provides a robust solution around BAO scales ($r_{\rm BAO} \sim 100h^{-1}$ Mpc). However, we observe deviations for separations below $r \sim 80h^{-1}$ Mpc. Both the perturbative CLPT and the "quasilinear" solution start to diverge from the simulation data and the other solutions, which becomes especially noticeable in the middle row panel where we focus on separations below $r = 40h^{-1}$ Mpc. On these smaller scales, the CLPT solution follows a trajectory similar to the quasi-linear solution up to $r \sim 11h^{-1}$ Mpc, below which it deviates the most within the nonlinear regime. The "BBKGY-linear" solution performs better than the previous two cases, tracking the evolution of the simulation data within 5% of accuracy up to separations of $r \sim 11h^{-1}$ Mpc across all redshift values, but it deviates in the intermediate and nonlinear regimes. Lastly, the fully nonlinear solution derived from Eq. (2) with $P_{\rm nonlin}(k)$ from Halofit closely mirrors the full nonlinear dynamics of dark matter particles in the simulation, achieving an accuracy of approximately ∼10% up to separation of $r \sim 1.1h^{-1}$ Mpc, for $z = 0$ and, $r \sim 1h^{-1}$ Mpc, for $z = 0.3$, 0.5. Our solution exhibits a consistent trend with redshift when compared to the simulation data, showing a gradual decrease in the $v_{12}(r,a)$ value at its minimum during earlier snapshots. We delve deeper into the analysis of this characteristic within the framework of various MG models.

For the remainder of the paper, unless explicitly specified otherwise, it is presumed that the solutions presented pertain to the "BBKGY-Halofit" method.

[2]https://github.com/wll745881210/CLPT-GSRSD.

B. MPV in MG theories

In our treatment of MG theories, the modifications to GR are contained in the linear power spectra from MGCAMB, which properly takes into account the modified gravitational interactions for a Hu-Sawicky $f(R)$-gravity, and the nDGP model. The nonlinear part of the solution, however, is generated from the standard ΛCDM-Halofit fitting formulas. This setting will be referred to as "BBGKY-Halofit" in our presentation.

The resulting v_{12} models are visualized in Fig. 2 in units of km s^{-1}, which, as done previously for the ΛCDM case, consists of three rows corresponding to three snapshots from the simulations: from top to bottom, $z = 0$, 0.3, 0.5. The rows labeled with the corresponding snapshot value showcase the trend of $v_{12}(r,a)$ in these MG models over the range of separations $r \in [0.05, 40]h^{-1}$ Mpc. Specifically, the six panels on the left illustrate the results for $f(R)$ variants (F5 and F6), while the six panels on the right depict the results for the nDGP variants (N1 and N5). The data points with associated errors represent the simulation outputs obtained directly calculating the projected velocity differences of pairs of dark matter particles. To facilitate comparison, we also present the simulation results for GR in all the figures, denoted by the solid points, as well as the corresponding Halofit solutions to Eq. (2), in black lines.

In each case, the bottom subpanel displays the ratio of the solution for $v_{12}(r,a)$ with respect to the corresponding MG model simulation, expressed as $\Delta v_{12} \equiv (v_{12} - v_{12,\rm sim})/v_{12,\rm sim}$. The shaded regions in these subplots represent the corresponding relative errors associated with the simulation data.

Starting with the plots which illustrate the full evolution of $v_{12}(r,a)$, we observe that the simulation data for the F6 (blue points) and N5 (magenta points) models closely track the evolution seen in the GR case (black points). This trend persists as we move from top to bottom in Fig. 2, indicating that our model captures the temporal evolution even in these non-ΛCDM scenarios.

Regarding our model for $v_{12}(r,a)$ (solid lines), we see how our solution from the BBGKY-Halofit model captures the trends of the simulation data in all cases and for all snapshots. For the case of Hu-Sawicki $f(R)$ gravity, we find that our model follows more closely the simulation data in the weaker version of the theory (F6, indicated by green lines and green points). For the F5 variant, we notice that our solutions deviate from the simulation data at the larger separations $r > 10$, 5, $1h^{-1}$ Mpc, for the snapshots $z = 0.5$, 0.3, 0, respectively. To better appreciate how the dynamics of pairwise velocities is captured by our model, we refer to the ratios Δv_{12} shown in the narrow subplots at each panel. Starting from the left side, or the $f(R)$ model, we notice a constant offset of the BBKGY-Halofit solution at large scales ($r \approx 40h^{-1}$ Mpc). This offset reaches $\Delta v_{12} \sim 10\%$ for the F6 case, and it is more prominent ($\Delta v_{12} \sim 20\%$) for the stronger variant of the model, F5.

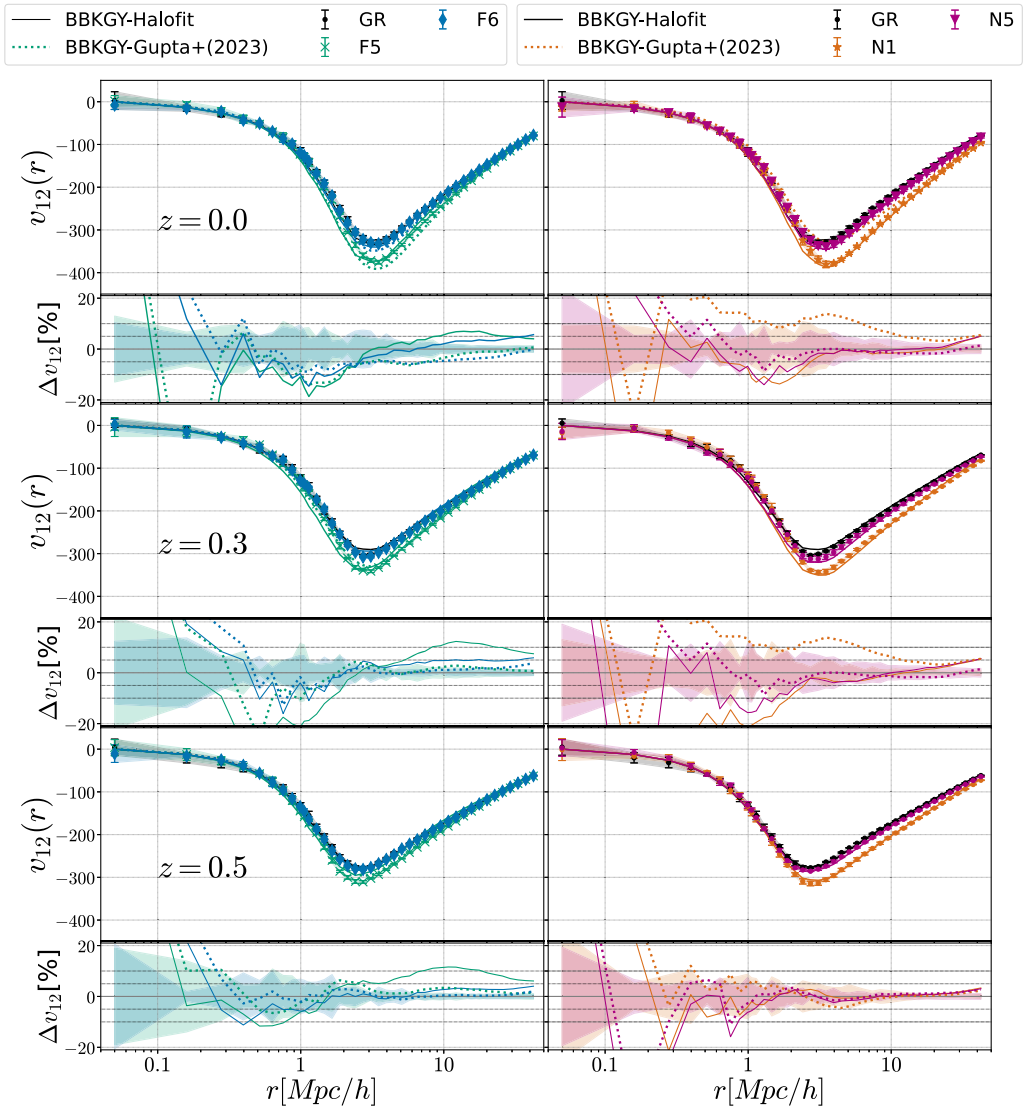

FIG. 2. Pairwise velocities, $v_{12}(r, a)$ in units of km s^{-1}, and models in MG theories. Points correspond to DM particles from the ELEPHANT runs, solid lines to the result from BBKGY-Halofit prediction, and dotted lines to the solution using Eq. (4), labeled as "BBKGY-Gupta(2023)". The results for the GR case are represented in black, the F5 model with turquoise, F6 in blue, N1 in orange and N5 in magenta.

In contrast, the solutions obtained with Eq. (4) or BBKGY-Gupta(2023), recover the expected values at these large separations.

Generally speaking, our model with the BBKGY-Halofit solution accurately captures the dynamics from the $f(R)$ simulations with better than 10% accuracy for separations of a few h^{-1} Mpc (between 2–10h^{-1} Mpc). However, as we approach the fully nonlinear regime or sub-megaparsec separations, there are noticeable deviations from the data, particularly for F5 at $z = 0.3$. The results from using the BBKGY-Gupta(2023) prescription perform better in all the cases mentioned above.

We notice how both solutions perform well for the $z = 0.5$ snapshot, achieving an accuracy of 10% or better for scales down to $r \sim 0.3(0.15)h^{-1}$ Mpc, for F5 and F6, respectively.

Turning to our nDGP solutions (right column of Fig. 2), we observe a better agreement between our model and the simulation data, for the specific case of the BBKGY-Halofit solution. In each sub-panel presenting the ratio Δv_{12}, we see that our prediction initially shows an offset of $\sim$10% at 40h^{-1} Mpc separations but then converges to the result from direct calculation in the simulation data for separations between a few and 10h^{-1} Mpc. At $z = 0$ our model captures the nonlinear evolution of $v_{12}(r, a)$ with 10% accuracy or better for pairs separated between 3–40h^{-1} Mpc. This level of accuracy is similarly observed at $z = 0.3$, and it improves further at $z = 0.5$, where we

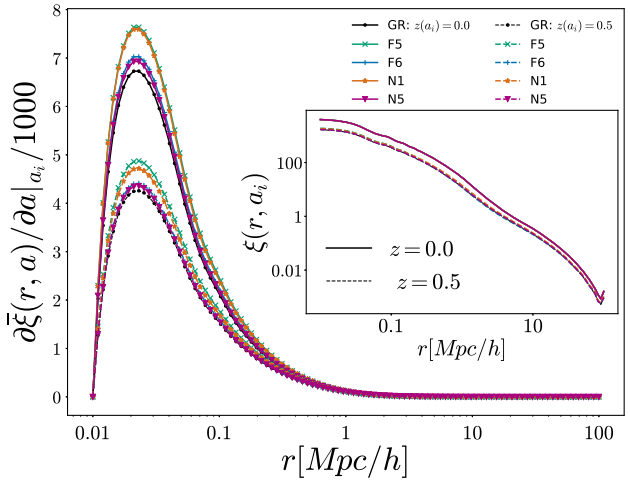

FIG. 3. Source (left-hand side) term of Eq. (2) with a focus on the time derivative of the volume-averaged correlation function part, for the different gravity models (GR, F5, F6, N1, and N5), and for $z = 0$ (solid lines), $z = 0.5$ (dashed lines). As an inset plot we show the factor multiplying $\partial\bar{\xi}/\partial a$, for the same models, z values, and r range.

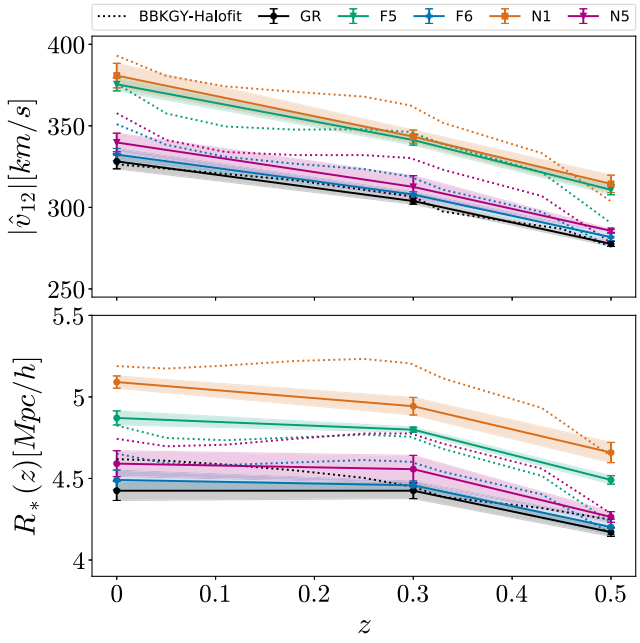

FIG. 4. Prediction of the maximum value of the infall pairwise velocity, $|\hat{v}_{12}(z)|$, and the stable-clustering crossing scale, R_*, as function of redshift. The expectation of a decreasing function for higher values of z is present for all models; however, we notice differences compared to GR.

achieve an agreement better than 10% for scales $r \geq 1h^{-1}$ Mpc. For our model using the BBKGY-Gupta (2023) prescription (shown in dotted lines) we notice that these solutions under-perform in comparison to the BBKGY-Halofit solution, particularly for $z = 0.3$, at which the pairwise velocities offset by 10% or more the direct calculation from our simulations, for separations $r \sim 5h^{-1}$ Mpc.

To understand better where these differences among gravity models come from, in Fig. 3 we illustrate the various components of the source term (left-hand side) of Eq. (2). The clustering itself, denoted by $\xi(r, a)$, exhibits minimal variation among gravity models (depicted in the inset figure for redshift values, $z = 0$, and 0.5, for variants F5, F6, N1, N5, and the GR case). However, its time evolution, represented by $\partial\bar{\xi}/\partial a$, reveals notable differences across models.

Specifically, the more pronounced modifications of GR, N1, and F5 exhibit a maximum deviation of approximately 13% from GR, at $z = 0$ (shown in solid lines), in contrast to the milder variants (N5 and F6), which deviate around 3–4% from the GR prediction at their maximum.

Notably, while at $z = 0$, the values for $\partial\bar{\xi}/\partial a$ for models F6 and N1 coincide, these models display different values at $z = 0.5$. In this case, their relative deviations from GR are approximately 11% and 14%, respectively, while the N5 and F6 variants show deviations of around 2%–4% compared to the GR prediction.

C. Signatures of MG in the MPVs

Comparing pairwise dynamics across different gravity models reveals interesting characteristics. As we can see in Fig. 2, the minimum value of $v_{12}(r, a)$ undergoes variations based on the gravity model. Specifically, for the stronger deviations from GR, $v_{12}(r, a)$ reaches a more pronounced minimum compared to scenarios involving weaker modifications of gravity or adhering to the GR framework.

To quantify this effect, we present the maximum value of $|v_{12}(r, a)|$, denoted as $|\hat{v}_{12}|$, as a function of redshift, z, in the top row of Fig. 4. As anticipated, during earlier cosmic times, relative velocities attain smaller magnitudes in comparison to the present epoch. Across all cases displayed in the top row of Fig. 4, there is a consistent trend toward smaller $|\hat{v}_{12}|$ (indicated by shallower curves for $v_{12}(r, a)$ in earlier snapshots, as seen in Fig. 1–2). The noteworthy observation lies in how this value varies across distinct gravity models.

First we focus on the values from the simulation data. These are represented by the error bar points at each snapshot value: $|\hat{v}_{12}|(z = 0, 0.3, 0.5)$. The errors express the standard deviation relative to the mean calculated from all realizations, also shown in the respective shaded regions. The distinctions between the values of $|\hat{v}_{12}|$ for GR and MG models become quite apparent. While the value of $|\hat{v}_{12}(z)|$ for the weaker modifications of GR (the variants F6 and N5 denoted by blue crosses and purple diamonds, respectively) closely tracks the trend of GR (indicated by black circles), we see that for the more pronounced MG variants (F5 and N1, represented by green triangles and orange squares, respectively) $|\hat{v}_{12}(z)|$ exhibits significant deviations from the GR values. In particular, at $z = 0$, the relative difference, defined as

$\Delta|\hat{v}_{12}| \equiv (|\hat{v}_{12,\mathrm{MG}}|/|\hat{v}_{12,\mathrm{GR}}| - 1)$, reaches 16% (or an increment of 52 km s^{-1}), for the N1 case. Similarly, the F5 variant has $\Delta|\hat{v}_{12}| \sim 14\%$ with respect to the GR value (an increment of ∼47 km/s). For the models N5 and F6, this deviations are negligible with respect of the uncertainties ($\Delta\hat{v}_{12} \approx 3.6, 1.2\%$, respectively). For earlier snapshots, the deviation between N1 or F5 and GR is of the same order of magnitude: $\Delta|\hat{v}_{12}| \approx 12$–$13\%$. Importantly, these deviations between gravity models are larger than the uncertainties in $\Delta|\hat{v}_{12}|$ from the simulation data. Conversely, for the weaker modifications of GR, as expressed in the F6 and N5 variants, the relative deviations are contained within the data uncertainties. We add the solutions from our model, shown as dotted lines.

For the GR case, and the N1 and F5 variants, our prediction for $|\hat{v}_{12}|$ agrees within the data uncertainties, except for N1 at $z = 0.3$, while our prediction for $|\hat{v}_{12}|$ in the case F6 and N5 presents an offset with respect to the simulation data. However, in all cases we recover the two main trends shown in our data: a decreasing value of $|\hat{v}_{12}|$ for earlier snapshots, and more importantly, the relative increment with respect to GR in the different MG scenarios. In particular, we recover the maximum deviation for the N1 variant, followed by the F5 case, then the N5 variant, and lastly, the F6 model.

Another interesting aspect to consider is the scale at which each model transitions into the stable clustering regime. We denote this specific scale as R_* and defined to be such that $aR_*H(z) - v_{12}(R_*) = 0$. To illustrate this point, in Fig. 5, we explicitly show the values for $-v_{12}(r, z = 0)$ for all the models under study, together with the Hubble velocity, rH_0 (dashed line). In vertical dotted lines we indicate the value of r at which both lines cross each other, in other words, the value for $r = R_*$ for each model.

As previously explained, $v_{12}(r, a)$ is dominated by the Hubble flow at large separations, gradually transitioning into the stable clustering regime as pairs of objects draw closer ([29,30]). However, the scale R_* at which this transition takes place varies depending on the underlying gravity theory. The outcomes of this analysis are presented in the bottom panel of Fig. 4.

In the bottom panel of Fig. 4 we show the stable-clustering crossing scale $R_*(z)$ for each gravity model. The values from our simulation data are shown in solid lines with error bars and the corresponding model prediction, in dotted lines. An interesting result is how this scale increases for the MG models that deviate more prominently from the GR case. We recover a similar behavior as the variation of $|\hat{v}_{12}|$ with the gravity model, namely, that the strongest deviation in the value of R_* is found for the N1 variant, followed by the F5 case, the N5 and lastly, the F6 case. Our model predictions lie outside the data uncertainties. Nevertheless, we recover the data trends for each one of the MG cases.

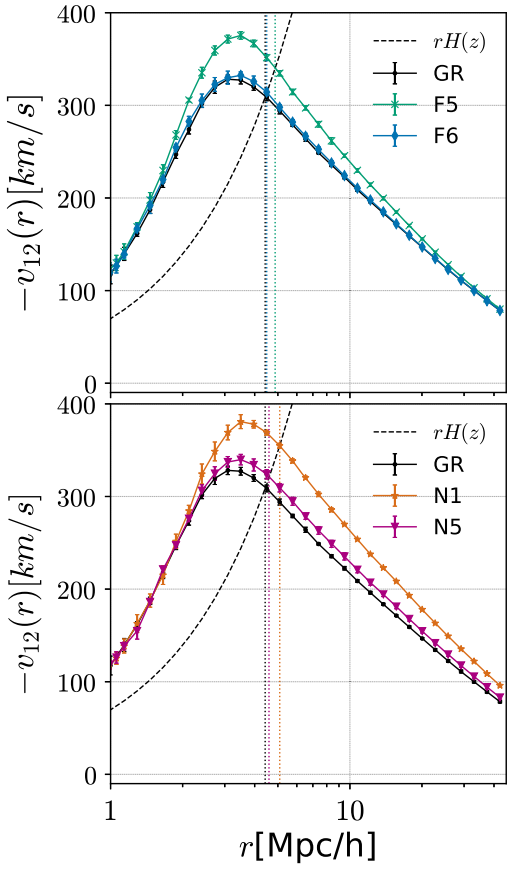

FIG. 5. Stable-clustering crossing scale, R_*, at $z = 0$ for the different models used in this work. In both panels we show the term $-v_{12}(r)$ for each model, and the Hubble flow $rH(z)$, which is identical in all models. The data points represent the values extracted from the simulation data with error bars displaying the variance from five independent box realizations. In the top panel we show the $v_{12}(r, a)$ for the F5 and F6 variants of $f(R)$-gravity, and the bottom panel shows the N1 and N5 variants of the nDGP model.

IV. DISCUSSION

In this paper we have presented the modeling for the evolution of pairwise velocities, for the linear, quasilinear, and fully nonlinear regime. Our model relies on the proper solution of the clustering in said regimes, and at its core, it sits on the pair-conservation equation as derived from the BBGKY hierarchy. The elegance of this approach allowed us to test its validity beyond the standard framework of GR and ΛCDM.

In Fig. 1 we have shown the solution from Eq. (2) and compared it against known approximations, and also against the direct calculation of the projected relative velocity differences of pairs in our N-body simulations.

In particular we see that the fully consistent solution of Eq. (2), using the Halofit template for the clustering (BBKGY-Halofit), provides excellent agreement with the ΛCDM simulation data throughout all the range

($r \in [0.05\text{–}140]h^{-1}$ Mpc), and importantly so, in the sub-megaparsec regime.

It is essential to acknowledge the limitations of our direct estimation from simulation data, with the smallest resolved scales being at $r = 0.05h^{-1}$ Mpc. A recent study [60] delved into the accuracy of pairwise velocities in N-body simulations, albeit in a scale-invariant Einstein-de-Sitter cosmology ($\Omega_{\rm tot} = \Omega_m = 1$). Despite this limitation, their findings revealed that the direct calculation of projected velocities between particle pairs in the simulation and the estimation using the 2PCF in the conservation equation are equivalent. Importantly, their simulations reached smaller scales than those covered in our work, which encompasses the range of scales presented in our analysis.

While perturbative solutions, such as CLPT, were proposed to provide accurate solutions in the BAO regime, they understandably do not match the evolution of the $v_{12}(r,a)$ below several tens of h^{-1} Mpc. The ansatz proposed by the authors of [28] (labeled in our solutions as "quasilinear") shows a better performance in comparison to the perturbative treatment of CLPT. While the behavior of $v_{12}(r,a)$ for CLPT shows an nonphysical turn toward positive values of $v_{12}(r,a)$ in the range of $r \leq 10h^{-1}$ Mpc, the quasilinear approximation correctly shows the tendency to a decreasing value in the $v_{12}(r,a)$ in such regime. Importantly too, we can notice how the quasilinear converges to the solution of the full BBKGY hierarchy using as an input a linear model for the 2PCF (a solution we named BBKGY-linear). This result shows the power of consistently solving Eq. (2), and its ability to provide better results than with other approximations.

In the bottom panel of Fig. 1 we show that our numerical solution is within 10% accuracy for the three snapshots, all the way down to $r \approx 1h^{-1}$ Mpc. In the particular case of $z = 0.5$, however, our numerical solution is consistent with numerical errors (which are below the 10% lines) even at separations of $r \sim 300\text{–}400$ kpc$/h$. For the intermediate snapshot, $z = 0.3$, this is achieved up to $r \sim 1h^{-1}$ Mpc, and for $z = 0$, up to $r \sim 2h^{-1}$ Mpc.

The underlying assumptions for the validity of Eq. (2) are tied to the conservation of pairs of dark matter particles in an expanding Universe (see chapter IV of [27] and the discussion in [31]). We check whether the solutions can be applied to cosmological models beyond ΛCDM. In particular, we have investigated the case when we relax the assumption of general relativity as the underlying law of gravity at all scales.

In Fig. 2 we can see the remarkable agreement between the solution of Eq. (2) and the simulation data obtained for the MG scenarios described in Sec. II. In this case we present the results of fully solving the BBKGY hierarchy Eq. (2) with the Halofit prescription to obtain the nonlinear power spectrum, $P_{\rm nl}(k,z)$, from the linear power spectrum in the MG scenarios under consideration, $P_{\rm lin,MG}(k)$. While, as mentioned previously, the Halofit ingredients were calibrated to match the nonlinear clustering in ΛCDM, our $P_{\rm lin,MG}(k)$ properly takes into account the modified gravitational interactions for a Hu-Sawicky $f(R)$-gravity, and the nDGP model.

In the first MG scenario, the Hu-Sawicki $f(R)$ theory, we found a constant shift between our solution and the simulation data, for pairs separated a few tens of h^{-1} Mpc. While one plausible explanation for this deviation might stem from the absence of a well-defined large-scale limit for pairwise velocities, as discussed in [1], an alternative hypothesis implicates the potential influence of the absent effective screening mechanism in this intermediate regime [at approximately ($r = 30h^{-1}$ Mpc)]. The observed constant shift prompts speculation about the nuanced interplay between the characteristics of the $f(R)$ theory and the larger-scale dynamics, necessitating further investigation to discern the precise origins of this discrepancy.

Note however that this offset is not present when we use the solution from [59] for the $f(R)$ model. Instead, the regime of applicability of our model is extended using the BBGKY-Gupta solution in our prediction for $v_{12}(r,a)$. We recall that the response function in Eq. (4) was calibrated against the ELEPHANT suite of simulations, to provide a proper modeling for the nonlinear clustering in the MG scenarios under consideration.

On the other hand, for the nDGP case (bottom panel of the second row of Fig. 2) we show that our solution properly models the dynamics for pairs separated $r \gtrapprox 2h^{-1}$ Mpc for the snapshots $z = 0$, 0.3, and for pairs separated at $r \gtrapprox 1h^{-1}$ Mpc, for $z = 0.5$. We compare our model against the numerical results obtained from the simulation data, and shown as shaded regions around the value $\Delta v_{12}(r,a) \equiv [v_{12} - v_{12,\rm sim}]/v_{12,\rm sim}$. This level of agreement is achieved with our BBKGY-Halofit prediction. In the case of the BBKGY-Gupta(2023) solution the results deviate beyond the propagated error range of the simulation data across all values of r, in the specific case of N1, at the snapshots $z = 0$, 0.3, but we obtained a better match for the value $z = 0.5$. The solution for the N5 variant from the BBKGY-Gupta(2023) was found more consistent with the uncertainties from the simulation particles in the three z values. We speculate that this can be an effect of the offset in their response functions (Fig. 2 of [59]) for the specific case of N1.

In all the cases that we discussed, both in GR and MG cosmologies, we find better agreement between our solutions and the simulation data for the higher redshift snapshot ($z = 0.5$), in comparison to the subsequent values, $z = 0.3$, 0. This can be attributed to the fact that the more recent snapshots represent highly nonlinear stages of the evolution of the Universe, therefore, the scale at which our prediction is accurate decreases with the redshift.

From examining the left hand side term of Eq. (2), we conclude that it is the time evolution of $\bar{\xi}$ what determines the dependence of $v_{12}(r,a)$ on the gravity model.

A perhaps more interesting result can be seen in the results shown in Fig. 4, where we study the differences in the dynamics of $v_{12}(r,a)$ between the various gravity prescriptions. We focus on two distinct features, the value of $v_{12}(r,a)$ at its minimum as a function of redshift, $\hat{v}_{12}(z)$, and the scale at which the pairs enter the stable clustering regime, $R_*(z)$, instead of being dominated by the Hubble flow. This scale is defined by the ratio of the streaming velocity to the Hubble expansion. It is important to remember that the modifications of the underlying gravity model are taken into consideration only at perturbation level in the ELEPHANT suite of simulations, keeping the same background as in GR for all the models under scrutiny. In other words, the effect of changes in the expansion rates that such models have (see for instance [61–63] where the specific case of $f(R)$-gravity theories in the cosmological context is discussed) are not considered in our simulations. Therefore, the differences found in the value of $R_*(z)$ express changes arising only from gravitational clustering in these MG scenarios, which helps to pinpointing changes attributed to the modified force law rather than by the modified expansion dynamics. The same claim is valid for the maximum value of $|v_{12}(z)|$, denoted as $|\hat{v}_{12}(z)|$, which encodes the enhanced infall velocities of pairs of galaxies in this alternative gravity models, with respect to GR.

Interestingly, we see a connection between the effect of the strength of the modification of gravity and the changes in the values of $|\hat{v}_{12}(z)|$ for a given z: $\Delta|\hat{v}_{12}| \equiv |\hat{v}_{12,\mathrm{MG}}|/|\hat{v}_{12,\mathrm{GR}}|$. The stronger modification of GR in the nDGP model, the case N1, displays the larger difference $\Delta|\hat{v}_{12}|$, followed closely by the F5 case of the $f(R)$ model.

These findings point to a distinct and recognizable signature from modifications of gravity on cosmological scales, which can potentially help detect the clear effect predicted by the implementation of these models, supporting the results presented in the letter [33], where different statistics for the pairwise velocities were analyzed. In that work, the authors focus on the amplitude of σ_{12}, the line-of-sight centered pairwise dispersion, also derived under the BBKGY formalism. A direct comparison to their results is not possible, as their analysis was based on the halo occupation distribution (HOD) mock galaxies, while we have kept our analysis on the dark matter particles, for which we are guaranteed that the conservation of pairs is fulfilled throughout cosmic history in the different snapshots we analyzed. However, some indirect comparison can be made as a part of the signal in σ_{12} that originates, in fact, from $\Delta v_{12}(r,a)$. Their results showed an increase in the amplitude of σ_{12}, for F5 with respect to GR, of approximately 25% at separations of $r = 1h^{-1}$ Mpc and $r = 5h^{-1}$ Mpc, the two cases probed in their analysis. This reinforces the primary finding that pairwise velocities serve as a potent tool for assessing the validity of general relativity (GR) on cosmological scales.

V. CONCLUSIONS

In summary, this study has outlined a robust methodology for accurately computing pairwise velocities across a wide range of regimes, encompassing linear, mildly nonlinear, and fully nonlinear stages. We have demonstrated that by adequately considering the clustering aspects and their temporal evolution, our approach can effectively predict the mean pairwise velocities (MPVs) within the range covered by our clustering model. Our analysis relies on the fundamental equation derived from the BBGKY hierarchy and employs nonlinear power spectrum models. Through Fourier transformation, we obtain the nonlinear two-point correlation function $\xi_{\mathrm{nonlin}}(r,a)$, which serves as the input to our core equation.

It is important to emphasize that this approach does not necessitate simplifications or approximations to generate reliable predictions for $v_{12}(r,a)$.

Furthermore, we have shown that this model is applicable to gravity models other than GR. Specifically, we have established that by appropriately accounting for nonlinear clustering in these alternative gravity models, our equation can seamlessly provide predictions for the infall velocities of pairs in these modified gravity (MG) scenarios. This highlights the versatility and robustness of our methodology, making it suitable for a broader range of cosmological investigations.

Even more, the different MG scenarios have a particular imprint in the dynamics of in-fall velocities. We have shown that the physical scale at which the dynamics between pairs is dominated by their gravitational attraction, as opposed to being dominated by the Hubble flow (crossing scale in the stable-clustering regime, R_*), is distinctively affected by the MG families of theories we analyzed. As screening mechanisms are a relatively generic prediction of viable MG theories, detecting deviations in the pairwise dynamics as we have described them would be a signature of physics beyond GR.

Furthermore, the pairwise velocity dispersion (PVD), σ_{12}, appears in the first moment of the second BBKGY equation [24,33]. The analysis of PVD is a vital component of redshift space distortions (RSD) models. To harness the full potential of ongoing and future data collection cosmological surveys like DESI [64], Euclid [65], and 4MOST surveys (CRS [66], and 4HS [67]), we must push the boundaries of our current RSD models. An extension of our model could result in physically-motivated model for RSD that could be applicable to a variety of gravity theories.

However, as we delve into smaller separations, the interplay between baryonic physics and dark matter distribution becomes increasingly significant. Specifically, the effect of baryons on RSDs, cosmic density and velocity fields has been thoroughly investigated in [68] by employing comprehensive hydrodynamical simulations. Their findings reveal that the impact of baryonic matter on halo and galaxy velocities becomes notable only at very small

separations, typically in the order of kiloparsecs. In fact, for separation scales smaller than $r \sim 0.6h^{-1}$ Mpc, the deviation in the total matter power spectrum is anticipated to be less than 20%. Furthermore, over a broad range of distances spanning from $r \sim 1.6$ to $62h^{-1}$ Mpc, the overall amplitude of the power spectrum deviates in less than 1% when compared to DM-only simulations. Therefore, the impact of baryons on the velocities of the DM samples employed in our work remains negligible over the broad range of scales under consideration.

However, for a realistic detection of such signatures we need to consider a number of systematic effects. The most immediate one is that we have modeled the signal directly on the pairs of dark matter particles, which can be guaranteed to be a closed system therefore ensuring the conservation of pairs. Conversely, halos and galaxies evolve through mergers and accretion, leading to a number density that is a stochastic function of the underlying dark matter distribution—a relationship known as bias.

While on large scales, we can expect a linear bias relationship, we aim to describe the dynamics of streaming motions on a wide range of scales. Therefore, a nonlinear bias model is crucial to properly account for the dynamics of pairs at sub-megaparsec scales. Although the studies by [30,31] have laid the groundwork in this area, the scenario involving theories with scale-dependent growth, and therefore, a scale-dependent bias, needs further exploration. These are immediate steps we plan to tackle in a follow-up paper.

ACKNOWLEDGMENTS

The authors would like to thank Adi Nusser for useful discussions, and to Hans A. Winther for kindly providing us with MGCAMB version for specific forms of $\mu(a, k)$ and $\gamma(a, k)$ functions implementing our nDGP models. We would also like to thank our anonymous referee for their comments which improved the clarity and robustness of our work. The authors acknowledge the support of the Polish Ministry of Science and Higher Education MNiSW grant No. DIR/WK/2018/12, as well as the research project "VErTIGO" funded by the National Science Center, Poland, under agreement number 2018/30/E/ST9/00698. J. E. G. F. is supported by the Spanish Ministry of Universities through a María Zambrano grant with reference UP2021-022, funded within the European Union-Next Generation EU. J. E. G. F. acknowledge the IAC facilities and the personnel of the Servicios Informáticos Comunes (SIC) of the IAC. M. B. is supported by the Polish National Science Center through Grants No. 2020/38/E/ST9/00395, No. 2018/30/E/ST9/00698, No. 2018/31/G/ST9/03388 and No. 2020/39/B/ST9/03494.

[1] R. Scoccimarro, Redshift-space distortions, pairwise velocities, and nonlinearities, Phys. Rev. D **70**, 083007 (2004).
[2] A. Taruya, T. Nishimichi, and S. Saito, Baryon acoustic oscillations in 2D: Modeling redshift-space power spectrum from perturbation theory, Phys. Rev. D **82**, 063522 (2010).
[3] F. Bernardeau, S. Colombi, E. Gaztañaga, and R. Scoccimarro, Large-scale structure of the Universe and cosmological perturbation theory, Phys. Rep. **367**, 1 (2002).
[4] H. Gil-Marín, C. Wagner, L. Verde, C. Porciani, and R. Jimenez, Perturbation theory approach for the power spectrum: From dark matter in real space to massive haloes in redshift space, J. Cosmol. Astropart. Phys. 11 (2012) 029.
[5] M. Crocce and R. Scoccimarro, Renormalized cosmological perturbation theory, Phys. Rev. D **73**, 063519 (2006).
[6] A. Taruya, RegPT: Regularized cosmological power spectrum, Astrophysics Source Code Library, record ascl: 1404.012 (2014).
[7] R. E. Smith and R. E. Angulo, Precision modelling of the matter power spectrum in a Planck-like Universe, Mon. Not. R. Astron. Soc. **486**, 1448 (2019).
[8] R. Takahashi, M. Sato, T. Nishimichi, A. Taruya, and M. Oguri, Revising the halofit model for the nonlinear matter power spectrum, Astrophys. J. **761**, 152 (2012).
[9] A. J. Mead, J. A. Peacock, C. Heymans, S. Joudaki, and A. F. Heavens, An accurate halo model for fitting nonlinear cosmological power spectra and baryonic feedback models, Mon. Not. R. Astron. Soc. **454**, 1958 (2015).
[10] K. Heitmann, E. Lawrence, J. Kwan, S. Habib, and D. Higdon, The coyote universe extended: Precision emulation of the matter power spectrum, Astrophys. J. **780**, 111 (2014).
[11] H. A. Winther, S. Casas, M. Baldi, K. Koyama, B. Li, L. Lombriser, and G.-B. Zhao, Emulators for the nonlinear matter power spectrum beyond ΛCDM, Phys. Rev. D **100**, 123540 (2019).
[12] Euclid Collaboration, Euclid preparation: IX. EuclidEmulator2—power spectrum emulation with massive neutrinos and self-consistent dark energy perturbations, Mon. Not. R. Astron. Soc. **505**, 2840 (2021).
[13] G. Brando, B. Fiorini, K. Koyama, and H. A. Winther, Enabling matter power spectrum emulation in beyond-ΛCDM cosmologies with COLA, J. Cosmol. Astropart. Phys. 09 (2022) 051.
[14] F. Beutler, C. Blake, M. Colless, D. H. Jones, L. Staveley-Smith, G. B. Poole, L. Campbell, Q. Parker, W. Saunders, and F. Watson, The 6dF Galaxy Survey: $z \approx 0$ measurements of the growth rate and σ_8, Mon. Not. R. Astron. Soc. **423**, 3430 (2012).
[15] C. Howlett, A. J. Ross, L. Samushia, W. J. Percival, and M. Manera, The clustering of the SDSS main galaxy sample—II. Mock galaxy catalogues and a measurement

of the growth of structure from redshift space distortions at $z = 0.15$, Mon. Not. R. Astron. Soc. **449**, 848 (2015).
[16] R. Watkins, H. A. Feldman, and M. J. Hudson, Consistently large cosmic flows on scales of $100h^{-1}$ Mpc: A challenge for the standard ΛCDM cosmology, Mon. Not. R. Astron. Soc. **392**, 743 (2009).
[17] Y. Hoffman, O. Metuki, G. Yepes, S. Gottlöber, J. E. Forero-Romero, N. I. Libeskind, and A. Knebe, A kinematic classification of the cosmic web, Mon. Not. R. Astron. Soc. **425**, 2049 (2012).
[18] C. Howlett, L. Staveley-Smith, P. J. Elahi, T. Hong, T. H. Jarrett, D. H. Jones, B. S. Koribalski, L. M. Macri, K. L. Masters, and C. M. Springob, 2MTF—VI. Measuring the velocity power spectrum, Mon. Not. R. Astron. Soc. **471**, 3135 (2017).
[19] P. Ganeshaiah Veena, R. Lilow, and A. Nusser, Large-scale density and velocity field reconstructions with neural networks, Mon. Not. R. Astron. Soc. **522**, 5291 (2023).
[20] R. Lilow and A. Nusser, Constrained realizations of 2MRS density and peculiar velocity fields: Growth rate and local flow, Mon. Not. R. Astron. Soc. **507**, 1557 (2021).
[21] H. M. Courtois, A. Dupuy, D. Guinet, G. Baulieu, F. Ruppin, and P. Brenas, Gravity in the local Universe: Density and velocity fields using CosmicFlows-4, Astron. Astrophys. **670**, L15 (2023).
[22] R. B. Tully, E. Kourkchi, H. M. Courtois, G. S. Anand, J. P. Blakeslee, D. Brout, T. d. Jaeger, A. Dupuy, D. Guinet, C. Howlett, J. B. Jensen, D. Pomarède, L. Rizzi, D. Rubin, K. Said, D. Scolnic, and B. E. Stahl, Cosmicflows-4, Astrophys. J. **944**, 94 (2023).
[23] S. J. Turnbull, M. J. Hudson, H. A. Feldman, M. Hicken, R. P. Kirshner, and R. Watkins, Cosmic flows in the nearby universe from Type Ia supernovae, Mon. Not. R. Astron. Soc. **420**, 447 (2012).
[24] P. Peebles, *Principles of Physical Cosmology* (Princeton University Press, Princeton, NJ, 2019), Vol. 99.
[25] P. J. E. Peebles, The peculiar velocity field in the local supercluster, Astrophys. J. **205**, 318 (1976).
[26] M. Davis and P. J. E. Peebles, On the integration of the BBGKY equations for the development of strongly nonlinear clustering in an expanding universe, Astron. Astrophys. Suppl. Ser. **34**, 425 (1977).
[27] P. J. E. Peebles, *The Large-Scale Structure of the Universe* (Princeton University Press, Princeton, NJ, 1980).
[28] R. Juszkiewicz, V. Springel, and R. Durrer, Dynamics of pairwise motions, Astrophys. J. **518**, L25 (1999).
[29] A. J. S. Hamilton, P. Kumar, E. Lu, and A. Matthews, Reconstructing the primordial spectrum of fluctuations of the universe from the observed nonlinear clustering of galaxies, Astrophys. J. Lett. **374**, L1 (1991).
[30] R. K. Sheth, L. Hui, A. Diaferio, and R. Scoccimarro, Linear and non-linear contributions to pairwise peculiar velocities, Mon. Not. R. Astron. Soc. **325**, 1288 (2001).
[31] R. K. Sheth, A. Diaferio, L. Hui, and R. Scoccimarro, On the streaming motions of haloes and galaxies, Mon. Not. R. Astron. Soc. **326**, 463 (2001).
[32] R. Juszkiewicz, P. G. Ferreira, H. A. Feldman, A. H. Jaffe, and M. Davis, Evidence for a low-density universe from the relative velocities of galaxies, Science **287**, 109 (2000).
[33] W. A. Hellwing, A. Barreira, C. S. Frenk, B. Li, and S. Cole, Clear and measurable signature of modified gravity in the galaxy velocity field, Phys. Rev. Lett. **112**, 221102 (2014).
[34] A. P. Hearin, Assembly bias &redshift-space distortions: Impact on cluster dynamics tests of general relativity, Mon. Not. R. Astron. Soc. **451**, L45 (2015).
[35] M. Gronke, C. Llinares, D. F. Mota, and H. A. Winther, Halo velocity profiles in screened modified gravity theories, Mon. Not. R. Astron. Soc. **449**, 2837 (2015).
[36] M. F. Ivarsen, P. Bull, C. Llinares, and D. Mota, Distinguishing screening mechanisms with environment-dependent velocity statistics, Astron. Astrophys. **595**, A40 (2016).
[37] A. Bibiano and D. J. Croton, Pairwise velocities in the "Running FLRW" cosmological model, Mon. Not. R. Astron. Soc. **467**, 1386 (2017).
[38] G. Valogiannis, R. Bean, and A. Aviles, An accurate perturbative approach to redshift space clustering of biased tracers in modified gravity, J. Cosmol. Astropart. Phys. 01 (2020) 055.
[39] G. Dvali, G. Gabadadze, and M. Porrati, 4D gravity on a brane in 5D Minkowski space, Phys. Lett. B **485**, 208 (2000).
[40] W. Hu and I. Sawicki, Models of f(R) cosmic acceleration that evade solar system tests, Phys. Rev. D **76**, 064004 (2007).
[41] L. Amendola, R. Gannouji, D. Polarski, and S. Tsujikawa, Conditions for the cosmological viability of f(R) dark energy models, Phys. Rev. D **75**, 083504 (2007).
[42] L. G. Jaime, L. Patino, and M. Salgado, f(R) Cosmology revisited, arXiv:1206.1642.
[43] A. I. Vainshtein, To the problem of nonvanishing gravitation mass, Phys. Lett. **39B**, 393 (1972).
[44] J. Khoury and A. Weltman, Chameleon cosmology, Phys. Rev. D **69**, 044026 (2004).
[45] T. Clifton, P. G. Ferreira, A. Padilla, and C. Skordis, Modified gravity and cosmology, Phys. Rep. **513**, 1 (2012).
[46] S. Alam, A. Aviles, R. Bean, Y.-C. Cai, M. Cautun *et al.*, Towards testing the theory of gravity with DESI: Summary statistics, model predictions and future simulation requirements, J. Cosmol. Astropart. Phys. 11 (2021) 050.
[47] M. Cautun, E. Paillas, Y.-C. Cai, S. Bose, J. Armijo, B. Li, and N. Padilla, The Santiago-Harvard-Edinburgh-Durham void comparison—I. SHEDding light on Chameleon gravity tests, Mon. Not. R. Astron. Soc. **476**, 3195 (2018).
[48] A. Lewis, A. Challinor, and A. Lasenby, Efficient computation of cosmic microwave background anisotropies in closed Friedmann-Robertson-Walker models, Astrophys. J. **538**, 473 (2000).
[49] C. Howlett, A. Lewis, A. Hall, and A. Challinor, CMB power spectrum parameter degeneracies in the era of precision cosmology, J. Cosmol. Astropart. Phys. 04 (2012) 027.
[50] R. E. Smith, J. A. Peacock, A. Jenkins, S. D. M. White, C. S. Frenk, F. R. Pearce, P. A. Thomas, G. Efstathiou, and H. M. P. Couchman, Stable clustering, the halo model and non-linear cosmological power spectra, Mon. Not. R. Astron. Soc. **341**, 1311 (2003).
[51] J. Carlson, B. Reid, and M. White, Convolution Lagrangian perturbation theory for biased tracers, Mon. Not. R. Astron. Soc. **429**, 1674 (2013).

[52] H. Oyaizu, M. Lima, and W. Hu, Nonlinear evolution of $f(r)$ cosmologies. II. Power spectrum, Phys. Rev. D **78**, 123524 (2008).
[53] S. Alam *et al.*, Towards testing the theory of gravity with DESI: Summary statistics, model predictions and future simulation requirements, J. Cosmol. Astropart. Phys. 11 (2021) 050.
[54] K. Koyama, A. Taruya, and T. Hiramatsu, Nonlinear evolution of the matter power spectrum in modified theories of gravity, Phys. Rev. D **79**, 123512 (2009).
[55] W. Hu and I. Sawicki, Parametrized post-Friedmann framework for modified gravity, Phys. Rev. D **76**, 104043 (2007).
[56] A. J. Mead, J. A. Peacock, C. Heymans, S. Joudaki, and A. F. Heavens, An accurate halo model for fitting non-linear cosmological power spectra and baryonic feedback models, Mon. Not. R. Astron. Soc. **454**, 1958 (2015).
[57] G.-B. Zhao, Modeling the nonlinear clustering in modified gravity models. I. A fitting formula for the matter power spectrum of f(r) gravity, Astrophys. J. Suppl. Ser. **211**, 23 (2014).
[58] A. Hojjati, L. Pogosian, and G.-B. Zhao, Testing gravity with CAMB and CosmoMC, J. Cosmol. Astropart. Phys. 08 (2011) 005.
[59] S. Gupta, W. A. Hellwing, and M. Bilicki, Improved analytical modeling of the nonlinear power spectrum in modified gravity cosmologies, Phys. Rev. D **107**, 083525 (2023).
[60] S. Maleubre, D. J. Eisenstein, L. H. Garrison, and M. Joyce, Constraining accuracy of the pairwise velocities in *N*-body simulations using scale-free models, Mon. Not. R. Astron. Soc. **525**, 1039 (2023).
[61] L. G. Jaime, L. Patiño, and M. Salgado, Note on the equation of state of geometric dark energy in $f(r)$ gravity, Phys. Rev. D **89**, 084010 (2014).
[62] L. G. Jaime, M. Jaber, and C. Escamilla-Rivera, New parametrized equation of state for dark energy surveys, Phys. Rev. D **98**, 083530 (2018).
[63] M. Jaber, G. Arciniega, L. G. Jaime, and O. A. Rodríguez-López, A single parameterization for dark energy and modified gravity models, Phys. Dark Universe **37**, 101069 (2022).
[64] DESI Collaboration, The DESI Experiment Part I: Science, targeting, and survey design, arXiv:1611.00036.
[65] R. Laureijs *et al.*, Euclid definition study report, arXiv:1110.3193.
[66] J. Richard, J. P. Kneib, C. Blake, A. Raichoor, J. Comparat, T. Shanks, J. Sorce, M. Sahlén, C. Howlett, E. Tempel, R. McMahon, M. Bilicki, B. Roukema, J. Loveday, D. Pryer, T. Buchert, C. Zhao (CRS Team Collaboration), 4MOST Consortium Survey 8: Cosmology Redshift Survey (CRS), The Messenger **175**, 50 (2019).
[67] E. N. Taylor *et al.* (4HS Team Collaboration), The 4MOST hemisphere survey of the nearby universe (4HS), The Messenger **190**, 46 (2023).
[68] W. A. Hellwing, M. Schaller, C. S. Frenk, T. Theuns, J. Schaye, R. G. Bower, and R. A. Crain, The effect of baryons on redshift space distortions and cosmic density and velocity fields in the EAGLE simulation, Mon. Not. R. Astron. Soc. **461**, L11 (2016).